environments

MDPI

Article

A Fixed-Resistance Polarization Strategy for High-Performance Biofilm Cultivation and Electron Storage Enhancement in MFCs

Jianbo Jia *, Jiteng Hong, Xiaolong Xu and Changyu Liu

Jiangmen Key Laboratory of Synthetic Chemistry and Cleaner Production, School of Environmental and Chemical Engineering; Carbon Neutrality Innovation Center, Wuyi University, Jiangmen 529020, China; 464379327@qq.com (J.H.); xuxl@wyu.edu.cn (X.X.); wyuchemcyliu@126.com (C.L.)
* Correspondence: jbjiagu@163.com

Abstract

Microbial fuel cells (MFCs) are bio-electrochemical devices that simultaneously treat wastewater and recover energy. However, their power generation performance is limited by the biocatalytic activity of electroactive biofilms. In this study, a low-cost, high-performance electroactive biofilm formation method was developed by replacing conventional constant potential polarization, which needs a fixed-resistance polarization approach. Additionally, alternating intermittent polarization with dual anodes was implemented based on these biofilms to continuously induce electron storage behavior. Experimental results confirmed the feasibility of the proposed fixed-resistance polarization method for biofilm cultivation. Compared with the primary biofilms, the derived biofilms exhibited markedly enhanced startup efficiency and power generation performance. Specifically, the startup time decreased by 24.8% from 44.23 h, while bioenergy conversion efficiency improved from 69.72 ± 3.30% to 91.90 ± 3.51%. These performance enhancements were attributed to the superior electrochemical activity of the derived biofilms, as evidenced by increased maximum current density, higher anode capacitance, and broader electrochemical activity range. These characteristics remained stable throughout the biofilm iteration process. Moreover, dual-anode alternating intermittent polarization successfully induced continuous electron storage behavior, leading to enhanced organic matter removal and energy conversion. Under the optimized conditions, MFCs demonstrated notable improvements in electroactivity. This study revealed the regulatory mechanisms of polarization patterns on biofilm formation and operation, providing an experimental foundation for the large-scale application of MFCs in wastewater treatment and energy recovery.

Keywords: microbial fuel cells; electroactive biofilms; derived biofilms; intermittent polarization; electron storage

Check for updates

Academic Editor: Pedro E. Arce

Received: 26 June 2026
Revised: 10 July 2026
Accepted: 12 July 2026
Published: 13 July 2026

Copyright: © 2026 by the authors. Licensee MDPI, Basel, Switzerland. This article is an open access article distributed under the terms and conditions of the Creative Commons Attribution (CC BY) license.

1. Introduction

Microbial fuel cells (MFCs) have emerged as a promising bio-electrochemical technology that enables simultaneous wastewater treatment and renewable energy recovery through organic matter conversion catalyzed by electroactive microorganisms (Scheme S1). While demonstrating potential for low-energy wastewater processing, biosensing, and environmental remediation, the practical implementation of MFCs remains constrained by technical limitations including low power density and operational instability [1–3]. A critical bottleneck lies in establishing high-performance electroactive biofilms [4–6].

Derived biofilms—electrochemically active biofilms developed through iterative microbial selection from primary biofilms—generally exhibit superior electrocatalytic activity compared with their primary counterparts [7–9]. The conventional preparation strategies for derived biofilms predominantly rely on potentiostatic polarization, which enriches electroactive microorganisms and enhances metabolic activity through controlled anode potential maintenance. However, this method necessitates expensive potentiostats and complex operational protocols, hindering large-scale application [10]. As a cost-effective alternative, fixed-resistance polarization indirectly regulates anode potential through external resistance adjustment [11]. Nevertheless, its efficiency in driving derived biofilm formation and its fundamental mechanistic differences from potentiostatic approaches remain insufficiently characterized.

Intermittent polarization, characterized by periodic depolarization–repolarization cycles, has been reported to improve MFC power output by inducing electron storage behaviors in electroactive microorganisms [12–14]. Previous investigations of intermittent polarization have primarily focused on primary biofilms, leaving the performance characteristics of derived biofilms under such conditions poorly understood. A critical limitation of this approach was identified in prolonged depolarization phases, which disrupted metabolic continuity and reduced system efficiency and may even lead to complete biofilm detachment [12,15,16]. Consequently, balancing sustained polarization continuity with induced electron storage behavior has emerged as a key challenge for optimizing intermittently polarized MFCs.

To address these knowledge gaps, this study systematically investigated the feasibility of replacing potentiostatic polarization with fixed-resistance polarization during derived biofilm development for the cost-effective production of high-performance biofilms. Furthermore, a novel intermittent polarization protocol employing dual-anode alternating depolarization–repolarization was developed based on these derived biofilms. This innovative configuration maintained continuous polarization across the MFC system, providing the opportunity to mitigate the detrimental effects of depolarization phases.

2. Materials and Methods

2.1. Construction of MFC Reactor

The dual-chamber MFCs with fed-batch operation were constructed using cubic polymethyl methacrylate blocks. Each reactor contained coaxial cylindrical chambers (14 mL volume each) housing carbon felt electrodes: a cylindrical anode (0.6 cm diameter × 2.0 cm height) and a rectangular cathode (2.0 × 2.0 × 0.5 cm). The electrodes were separated by a cation exchange membrane (7 cm^2, CMI-7000, Membranes International, NJ, USA) with an inter-electrode distance of 2.0 cm. The electrical circuit was completed through a 1000 Ω fixed resistor connected to a digital multimeter (Keithley Instruments DMM6500, OH, USA) for continuous voltage monitoring, with data recorded at 1 min intervals. Temperature control was maintained at 30 ± 0.5 °C using a constant-temperature water bath. To provide a stable-pH environment for microorganisms, 50 mM phosphate buffer solution (PBS, pH = 7.4) was selected. The selected PBS was composed of 4.34 g/L Na_2HPO_4, 2.78 g/L KH_2PO_4, 0.31 g/L NH_4Cl, and 0.13 g/L KCl. The anolyte was supplemented with 1.0 g/L sodium acetate in 10 mL PBS, while the catholyte contained 10 mL PBS with 50 mM potassium ferricyanide (conductivity: 23.5 mS/cm) [17] to stabilize cathode potential [18]. Following sterilization, an anaerobic condition was established through 15 min nitrogen gas purging of the medium.

2.2. Formation of Primary Biofilms

The primary biofilm inoculum was collected from an artificial lake in Jiangmen, China. Immediately after collection, the inoculum was stored below 4 °C until use [19–21]. For triplicate primary biofilm formation (corresponding MFCs were named PB-MFCs), the inoculum supernatant was mixed with anolyte at a 1:1 ratio and allowed to settle for 24 h before being introduced into the anode chambers. Equal-volume catholyte was subsequently injected into the cathode chambers. All the solution was removed and replaced with fresh electrolyte when the output voltage dropped below 50 mV. Mature biofilms were established when three consecutive reproducible voltage peaks were achieved, at which point subsequent experiments were initiated. The duration between initial inoculation and first voltage peak detection was defined as the start-up period.

2.3. Formation of Derived Biofilms

Following the formation of the primary biofilms, two sequential protocols were implemented for secondary biofilm development. In the initial protocol, a pristine carbon felt anode was introduced into the anode chamber containing the primary biofilm. While maintaining the original external circuit connection, the blank anode was simultaneously connected through a separate pathway to an independent external resistor and cathode. This primary protocol was discontinued when it failed to induce secondary biofilm formation. A modified protocol was subsequently adopted in which the original circuit connection was disconnected and re-established with the blank anode. Following successful secondary biofilm formation, an identical procedure was iteratively applied to subsequent generations using the latest biofilm as the progenitor. The resultant biofilms generated through this iterative process (as illustrated in Figure 1) were collectively termed as the derived biofilms. All the derived biofilms were subsequently transferred to newly assembled MFC reactors for independent operation. These specialized configurations were defined as derived biofilm MFCs (DB-MFCs).

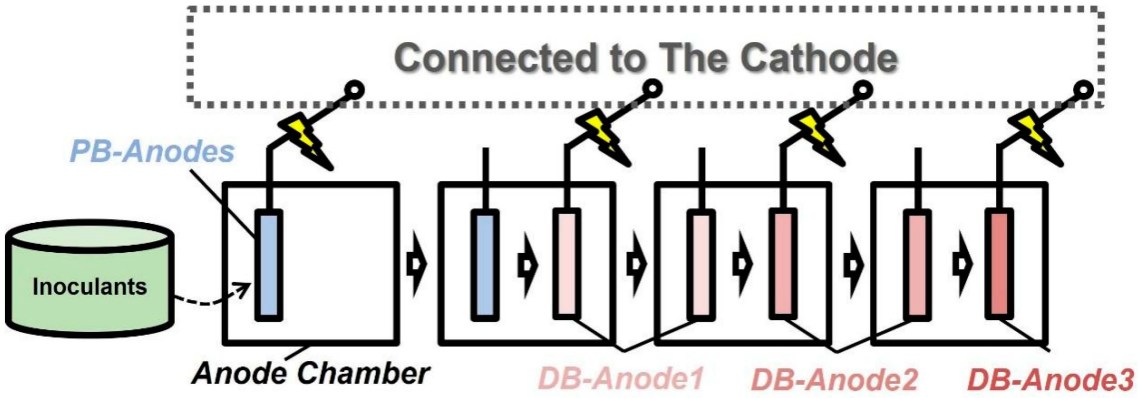


Figure 1. The iterative process of derived biofilms.

2.4. Alternating Intermittent Polarization

Following the derived biofilm's maturation, two DB-MFC anodes were integrated into a single reactor to establish a novel dual-anode configuration implementing alternating intermittent polarization. The bioanodes maintained a 2.0 cm inter-electrode spacing while being horizontally aligned relative to the shared cathode. Each anode was independently connected to distinct channels of a multi-channel potentiostat (CHI-1000C, CH Instruments, Shanghai, China) configured in two-electrode mode, where both anodes functioned as working electrodes and the cathode served as a counter/reference electrode. The alternating intermittent polarization protocol was implemented through automated macro

programming, systematically cycling between two operational states: one bioanode was maintained at open-circuit potential, while its counterpart underwent controlled polarization at −0.3 V (vs. cathode). These distinct electrochemical states were periodically exchanged at precisely alternating time intervals.

2.5. Analysis

The electrochemical activity of EABs was evaluated through cyclic voltammetry (CV) measurements conducted using a multi-channel potentiostat. Prior to testing, all MFCs underwent complete electrolyte replacement. The three-electrode configuration comprised: a working electrode (anode), a counter electrode (cathode), and a reference electrode (Ag/AgCl (saturated KCl), positioned 2.0 cm from the anode). All potentials were referenced against this Ag/AgCl electrode unless otherwise specified. CV scans were performed within a potential window of −0.8 V to 0.2 V at a scan rate of 20 mV/s. Anode capacitance was calculated using the formula: $C = \int IdV/(2v \times V)$, where $\int IdV$ represents the enclosed area of the CV curve, v denotes the scan rate, and V indicates the voltage window span [22–24]. The first derivative CV (DCV) was derived from the CV data by plotting the slope of each CV data point against the voltage (dI/dE). The DCV data points were fitted by a polynomial of degree 13 [25]. Polarization and power density curves were obtained through the variable resistance methodology [22]. Following electrolyte renewal and 4 h open-circuit stabilization, external resistances (100, 51, 10, 5.1, 1, 0.51, 0.33, and 0.10 kΩ) were sequentially applied in descending order with 15 min intervals between changes. Voltage measurements were recorded immediately before resistance switching. Current and power densities were calculated using established methods, normalized to the anode's geometric area (4 cm^2) [18]. Chemical oxygen demand (COD) concentrations were quantified using a portable analyzer (5B-3C, Lianhua Technology, China). Coulombic efficiency (CE) was calculated as $CE = 32 \times Q/4 \times F \times V \times \Delta COD \times 100\%$, where Q represents cumulative charge (C) from current–time integration, F denotes the faraday constant (96,485 C/mol), V represents anolyte volume (10.0 mL) and ΔCOD denotes the COD concentration difference (mg/L). Each experiment was performed in triplicate, and the results are expressed as mean ± standard deviation (SD).

3. Results

3.1. Formation of Primary and Derived Biofilms

The voltage–time curve of the primary biofilm during the startup period is shown in Figure 2a. After a 54 h inoculation period, the prepared PB-MFC entered the logarithmic growth phase, with the voltage reaching its peak (493.12 mV) in the following 5 h. Subsequently, the voltage of the PB-MFC rapidly decreased (<50 mV) due to the depletion of organic substrate. This indicated the completion of the first feeding cycle of the PB-MFC and the formation of the primary biofilm, with a startup time of 58.82 h. In the initial biofilm derivation protocol, both PB-MFCs and DB-MFCs were subjected to fixed-resistance polarization simultaneously and independently. Under this protocol, the activity of the primary biofilm was suppressed (the voltage of the PB-MFCs was <200 mV, which was significantly lower than its normal level (~500 mV)), and the derived biofilm was not successfully formed (DB-MFCs continuously output low voltage (<50 mV) for up to a week).

In the improved biofilm derivation protocol, polarization of PB-MFCs was interrupted, and only DB-MFCs were subjected to fixed-resistance polarization. Under this protocol, the derived biofilm was successfully formed (~36 h inoculation period and ~8 h logarithmic growth phase), and startup efficiency was enhanced: I. startup time was reduced by 24.8% to 44.23 h and II. peak voltage increased by 19.8% to 590.80 mV (Figure 2a). Using the improved biofilm derivation protocol, third- and fourth-generation biofilms were generated,

with no further enhancement in startup efficiency (startup time of 45.04 ± 3.09 h and peak voltage of 592.71 ± 9.52 mV, Figure 2b). Compared with these derived biofilms, PB-MFCs showed greater variability in performance metrics (startup time: 68.28 ± 9.96 h, and peak voltage: 489.21 ± 39.39 mV).

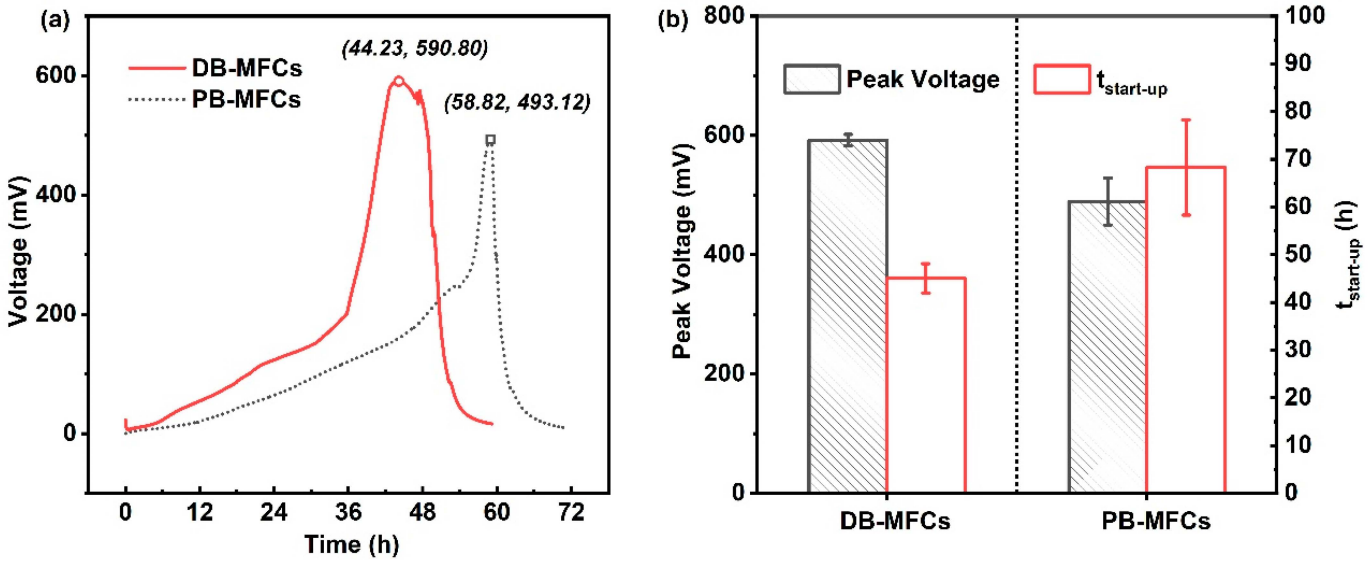


Figure 2. The growth curves of representative samples of primary biological membrane (PB-MFCs) and derivative biological membrane (DB-MFCs) during the startup period (**a**) and their startup efficiency (**b**).

3.2. Power Generation

Compared with PB-MFCs, superior power generation performance was demonstrated in DB-MFCs through four key metrics: (1) enhanced voltage responsiveness (faster recovery within feeding cycles) with sustained high output (Figure 3a); (2) reduced internal resistance (evidenced by lower polarization curve slopes (Figure 3b)); (3) increased maximum current density (9.82 ± 1.18 vs. 12.44 ± 1.99 A/m^2, 26.68% enhancement, Figure 3b); and (4) improved maximum power density (3.90 ± 0.13 vs. 5.47 ± 0.41 W/m^2, 40.26% increase, Figure 3c).

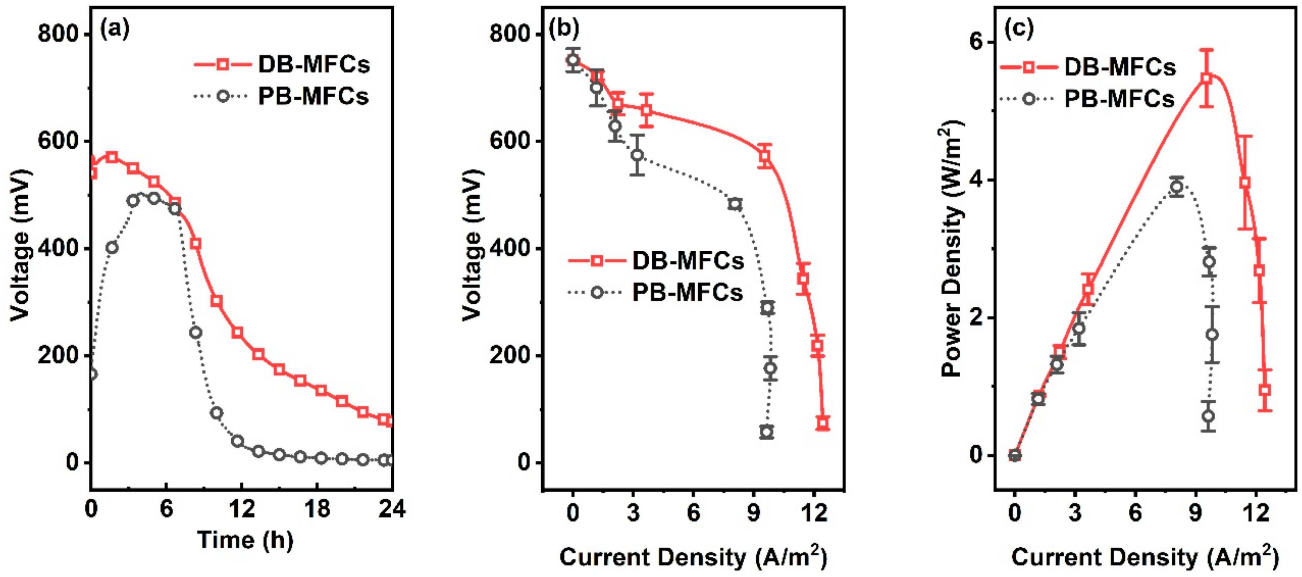


Figure 3. After startup, the voltage output of representative samples of primary biological membrane (PB-MFCs) and derivative biological membrane (DB-MFCs) (**a**), as well as the polarization (**b**) and power density curves (**c**).

Furthermore, compared with PB-MFCs, enhanced energy conversion efficiency was observed in DB-MFCs: (1) extended long-term power generation stability (LPGS, duration maintaining ≥80% peak voltage) [26] increased from 5.56 ± 0.56 to 7.37 ± 0.39 h (32.55% improvement, Figure 4a); (2) elevated cycle power output with total energy production per feeding cycle rising from 5.82 ± 0.41 to 10.62 ± 1.26 W (82.47% enhancement, Figure 4a); (3) improved bioenergy conversion efficiency demonstrated by coulombic efficiency increase from 69.72 ± 3.30% to 91.90 ± 3.51% (31.81% gain, Figure 4b); and (4) enhanced organic treatment capacity with COD removal rate improvement from 87.54 ± 2.47% to 89.62 ± 1.13% (2.38% increase, Figure 4b).

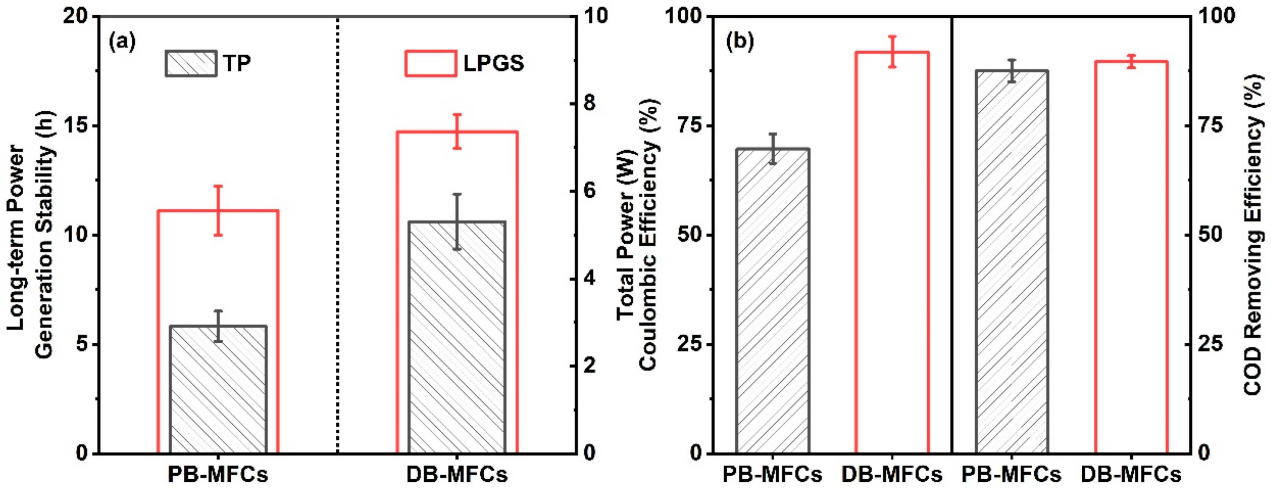


Figure 4. The total power obtained by each group of biological membranes in a single feeding cycle and long-term power generation stability (**a**), as well as the coulombic efficiency and COD removal rate (**b**).

3.3. Electrochemical Activity

Significant intra-group consistency in biofilm electroactivity was observed in DB-MFCs, as evidenced by nearly identical CV profiles and redox peak potentials (Figure 5a). In contrast, PB-MFCs exhibited substantial intra-group variations in electrochemical characteristics, as demonstrated by divergent CV curve morphologies and redox potential distributions (Figure 5b). Three key electrochemical improvements were demonstrated in DB-MFCs compared with PB-MFCs: (1) anodic capacitance increased by 68.57% (80.94 ± 42.57 vs. 136.44 ± 5.73 F/m^2, Figure 5c); (2) maximum current density improved 38.28% (11.31 ± 6.84 vs. 15.64 ± 8.70 A/m^2, Figure 5c); and (3) DCV revealed 66.17% expansion in electrochemical active range (78.50 ± 14.85 vs. 149.00 ± 36.01 mV, Figure 5d and Table 1).

Table 1. Electrochemical active range of derived biofilms (DB-MFCs) and primary biofilms (PB-MFCs).

MFCs	Electrochemical Active Range (V)
DB-MFC1	−0.369~−0.227
DB-MFC2	−0.324~−0.207
DB-MFC3	−0.366~−0.178
PB-MFC1	−0.280~−0.191
PB-MFC2	−0.271~−0.203
PB-MFC3	−0.316~−0.204

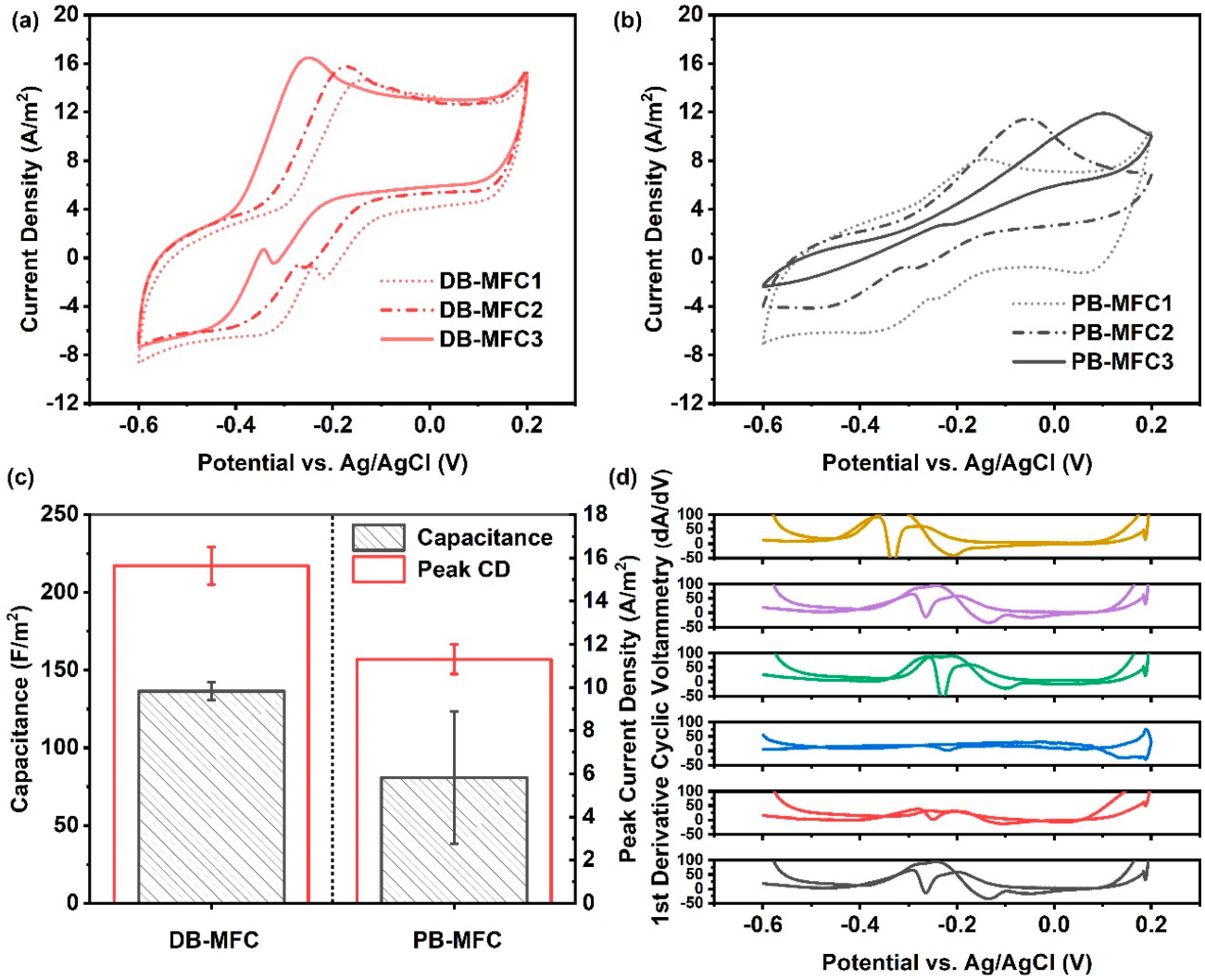


Figure 5. Cyclic voltammograms of the first- to third-generation derived biofilms (DB-MFCs, (**a**)) and the three replicate samples of primary biofilms (PB-MFC, (**b**)), with a potential window of −0.6 to 0.2 V, scan rate of 20 mV/s, and the solution medium being 50 mM PBS containing 1.0 g/L acetate; their capacitance and peak current density (**c**); and the first derivative plot of the cyclic voltammetry (smoothed), from top to bottom: DB-MFC1~3, PB-MFC1~3 (**d**).

3.4. Electricity Generation Under Alternating Intermittent Polarization

A dual-anode microbial fuel cell (D-MFC) was constructed using the derived biofilms. When operated under alternating intermittent polarization with 5 min alternating intervals, characteristic electron storage behavior was confirmed through current–time curve analysis, exhibiting the typical peak–valley–shoulder pattern observed in intermittent polarization studies (Figure 6a) [27]. Compared with single-anode MFCs (S-MFCs) operating under constant potential polarization (−0.3 V), D-MFCs demonstrated superior performance during 1 h operational cycles across four key metrics: (1) enhanced total power output ($12.17 \pm 0.86 \rightarrow 15.53 \pm 0.61$ W, 27.61% increase, Figure 6b); (2) improved charge production ($20.5 \pm 3.45 \rightarrow 24.42 \pm 0.95$ C, 19.12% gain, Figure 6b); (3) increased organic degradation capacity (COD removal: $16.54 \pm 2.51\% \rightarrow 21.56 \pm 1.44\%$, 50.35% improvement, Figure 6c); and (4) elevated energy conversion efficiency (coulombic efficiency: $85.86 \pm 3.82\% \rightarrow 94.03 \pm 2.63\%$, 9.52% enhancement, Figure 6c).

Systematic optimization of alternating intervals revealed a distinctive pattern (Figure 7a,b): all metrics initially increased, then decreased with prolonged intervals. Peak performance was achieved at 10 min alternating intervals: (1) maximum power output:

17.15 ± 0.51 W; (2) charge accumulation: 26.96 ± 1.12 C; (3) COD removal efficiency: 22.98 ± 1.59%; and (4) coulombic efficiency: 97.42 ± 3.01%. Following 72 h continuous operation under the optimized conditions, subtle electrochemical modifications were induced (Figure 7c): (1) cyclic voltammograms shifted slightly toward the upper-left quadrant; (2) enclosed area increased by 8.7%; (3) peak current density rose 6.4%; and (4) oxygen reduction potential remained stable (±30 mV variation).

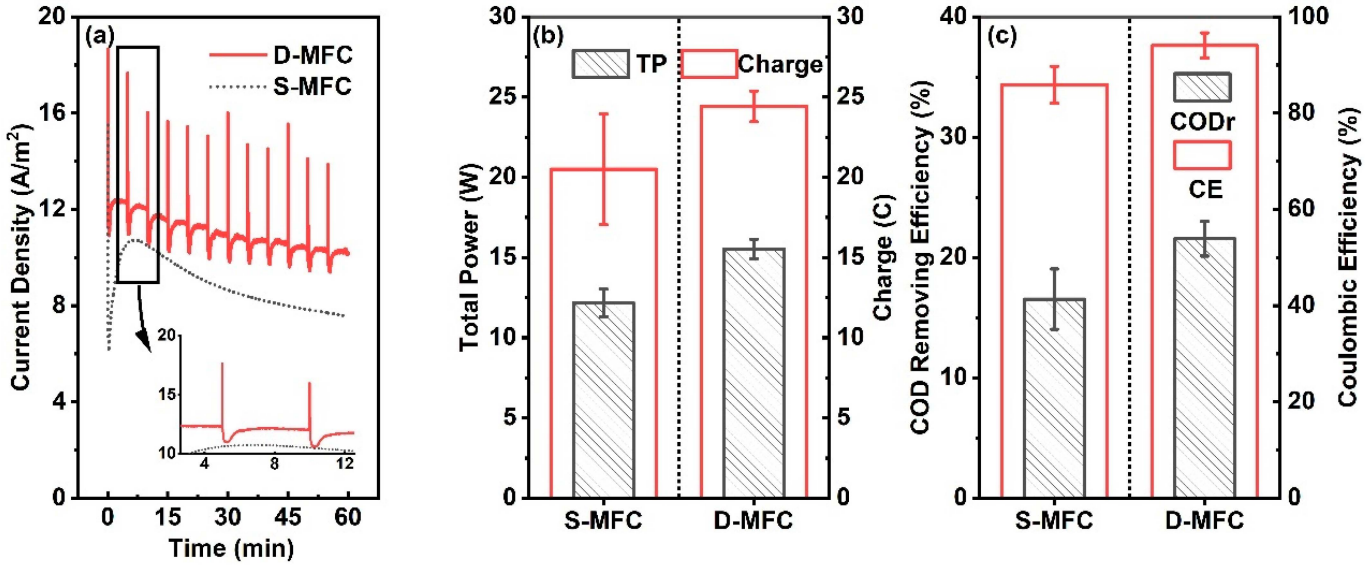


Figure 6. Current output of the dual-anode MFCs (D-MFC) operated under alternating intermittent polarization (−0.3 V constant potential or open circuit, with a 5 min interval) and single-anode MFCs (S-MFC) under constant potential polarization (−0.3 V) (**a**); total power and charge produced (**b**); and COD removal rate and coulombic efficiency (**c**) during this period.

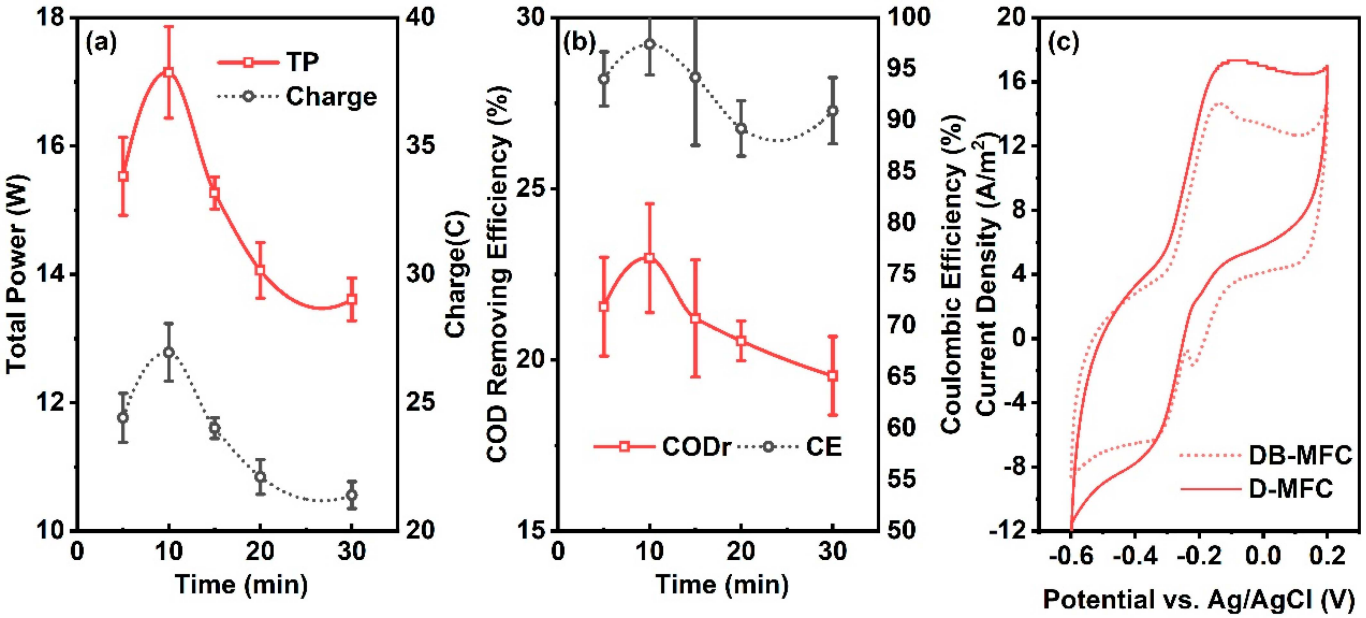


Figure 7. Performance under different alternating time intervals: total power and charge production (**a**); COD removal rate and coulombic efficiency (**b**). Changes in the electroactivity of the biofilm after 72 h of operation at the optimized alternating time interval (**c**).

4. Discussions

4.1. Formation of Biofilms Under Constant Resistance/Potential Polarization

Our study demonstrated the feasibility of replacing potentiostats with fixed resistors for electrode polarization during derived electroactive biofilm formation. We also found that strict potential control was crucial for the proper operation of the two anodes in a shared electrolyte. Initial protocols employing fixed-resistor polarization on both anodes resulted in suppressed metabolic activity of primary biofilms and inhibited derived biofilm development. This phenomenon was explained by the distinct mechanisms between potentiostatic and fixed-resistance polarization. In potentiostatic polarization, identical anode potentials were maintained between the primary biofilm-coated electrode and the blank electrode [8]. The established electroactive biofilm on the primary electrode adapted to this potential condition, which facilitated derived biofilm formation on the blank electrode.

In polarization with constant resistance, the anode potential was influenced by multiple factors including substrate [28], external resistance [11], and biofilm characteristics [29]. To maintain stable activity (high voltage output), electroactive microorganisms downregulate the anode potential by controlling electron transfer between themselves and the electrode. A significantly higher anode potential was observed on blank electrodes due to the absence of potential-regulating biofilms, potentially inducing oxidative stress in primary biofilms. This phenomenon consequently inhibited the metabolic activity of electroactive microorganisms. Under oxidative stress conditions [30], electroactive microorganisms preferentially colonized electrodes with a lower anode potential (those containing primary biofilms) [29,31,32], thereby suppressing colonization on blank electrodes.

Subsequent experimental evidence supported this interpretation: (1) Voltage recovery in PB-MFCs occurred within hours after blank electrode removal, indicating that primary biofilm inhibition was directly caused by fixed-resistance polarization of blank electrodes. (2) Under the modified experimental conditions, the cessation of primary biofilm polarization enabled electroactive microorganisms to utilize blank electrodes as unique electron acceptors, facilitating derived biofilm formation. This result demonstrated that sustained polarization of secondary biofilms prevented derived biofilm development. Although plausible explanations were proposed, further evidence supporting these theoretical premises was not obtained in this study, and the fundamental limitations remained unresolved. Maximum power point tracking—a technique for anode potential optimization—is commonly employed to regulate the formation and development of electroactive biofilms [33–35]. Therefore, implementing these strategies on blank electrodes during fixed-resistance polarization studies could potentially address these challenges in derived biofilm formation research.

4.2. Performance Under Fixed-Resistor Polarization

A systematic comparison of power generation characteristics was conducted between the pristine and derived biofilms under fixed-resistance polarization. Consistent with previous potentiostatic polarization studies, superior startup performance and power generation capability were observed in DB-MFCs, although no performance enhancement was achieved through biofilm iteration [7–9]. This investigation further revealed that DB-MFCs exhibited smaller intra-group performance variations than PB-MFCs, which aligned with their comparable startup characteristics and highly similar CV profiles. Furthermore, the enhanced energy conversion efficiency in DB-MFCs was substantiated through polarization curve analysis [36]. Compared with PB-MFCs, DB-MFCs demonstrated (1) lower open-circuit losses and activation losses (first segment of polarization curves) and (2) reduced ohmic losses (second segment), collectively contributing to improved organic degradation

and energy conversion. Although both MFC configurations exhibited rightward-shifted power density curves—indicative of mass transfer limitations [18]—the optimized organic degradation and energy conversion efficiency in DB-MFCs supported higher maximum current densities (12.44 vs. 9.82 A/m^2) and power densities (5.47 vs. 3.90 W/m^2). Notably, while comprehensive testing under practical conditions (e.g., continuous flow or real wastewater) was not conducted, this fixed-resistance polarization approach demonstrated, more directly than conventional potentiostatic systems, the potential of derived biofilms for wastewater-based power generation, particularly in real-world applications [8].

4.3. Potential Correlation Between Biofilm Electroactivity and Power Generation

The underlying mechanisms for stable performance enhancement in DB-MFCs were elucidated through systematic characterization of the biofilm's bio-electrochemical properties. Consistent with previous findings, derived biofilms exhibited CV profiles remarkably similar to those of *Geobacter sulfurreducens* biofilms, highlighting the dominance of this electroactive species [8]. However, this investigation revealed two novel aspects: (1) substantial bio-electrochemical variability among primary biofilm replicates and (2) bio-electrochemical stability during biofilm iteration processes. *G. sulfurreducens*, a model electroactive microorganism, has been extensively studied for its capacity to develop dense, uniformly distributed biofilms with high conductivity [27,32,37]. The dominance of such species demonstrated that sustained dominance establishment through biofilm succession constitutes an effective methodology for engineering high-performance electroactive biofilms [38–40]. The resultant bio-electrochemical optimization was ultimately correlated with enhanced power generation capabilities.

Quantitative analyses demonstrated three key improvements in derived biofilms compared with their pristine counterparts: (1) enhanced electron transfer capacity (15.64 vs. 11.31 A/m^2); (2) increased anodic capacitance (136.44 vs. 80.94 F/m^2); and (3) broader, yet more concentrated, electrochemical active ranges (149.00 vs. 78.50 mV). These observations suggested the upregulated expression of diverse redox enzymes in derived biofilms, enabling efficient electron transfer across wider anode potential ranges—a critical factor explaining the enhanced power generation [25,41]. Notably, while PB-MFC replicates showed significant CV profile variations, their peak current densities remained comparable, with primary electrochemical differences being capacitance-related. Although no direct biofilm structural characterization was conducted, the established correlation between capacitance improvements and performance metrics implied optimization during biofilm formation. The result aligns with previous reports linking capacitance to biofilm architecture [22–24], suggesting electrode capacitance modulation as a key mechanism for bio-electrochemical performance enhancement.

4.4. Feasibility of Alternating Intermittent Polarization

The feasibility of enhanced power generation using dual-anode MFCs (D-MFCs) under alternating intermittent polarization was preliminarily demonstrated. Consistent with previous studies, electron storage behavior was induced in electroactive microorganisms through intermittent polarization, which improved organic degradation and energy conversion efficiency, thereby enhancing MFC performance [12–14]. However, further improvements were achieved in this study through continuous system polarization enabled by alternating electrode operation. Compared with conventional intermittent polarization systems, two potential advantages were identified: (1) reduced hydraulic retention time and (2) enhanced energy conversion efficiency. While conventional intermittent systems can provide higher instantaneous power output during polarization phases, their mandatory open-circuit periods extended treatment duration. More critically, open-circuit conditions

risked promoting non-electrogenic species proliferation (e.g., methanogens) [42], thereby reducing energy conversion efficiency. The alternating polarization strategy ensured continuous system polarization by maintaining at least one anode in operational status, increasing substrate utilization opportunities for electroactive microorganisms.

A key limitation of the proposed system was identified: equal polarization and open-circuit durations were required to maintain continuity, unlike in conventional intermittent systems, which permit independent optimization of these parameters [12–14]. However, this constraint can be mitigated through multi-electrode configurations—a promising direction for future research that simultaneously highlights the technology's scalability. Through systematic optimization, a characteristic performance pattern was revealed (Figure 7a,b): all metrics initially increased, then decreased with extended intervals. The 10 min interval demonstrated optimal performance, potentially explained by: (1) insufficient stimulation of electron storage mechanisms (at <10 min, resembling continuous polarization) and (2) prolonged metabolic disruption (at >10 min) inhibiting electron transfer. Notably, this optimal interval differed significantly from previous reports (10 min vs. 10 s) [12], possibly due to: (a) distinct inoculum sources yielding varied biofilm properties; (b) biofilm development under constant resistance rather than intermittent polarization; and (c) electrode interaction effects in multi-anode systems.

Following 72 h operation under optimized conditions, significant electrochemical improvements were observed (Figure 7c). The leftward CV shift suggested improved substrate supply, while unchanged redox potentials indicated conserved electron transfer mechanisms [43,44]. Although the potential changes in biofilm performance under alternating intermittent polarization were not examined, these modifications suggested electrochemical improvements under alternating polarization—which can be very distinct from traditional intermittent systems—further demonstrating the technology's potential.

5. Conclusions

The feasibility of employing fixed-resistance polarization as an alternative to potentiostatic polarization during derived biofilm formation was demonstrated, providing new insights into electroactive biofilm development under different polarization regimes. The performance of derived biofilms was systematically investigated under fixed-resistance polarization, highlighting its critical role in developing stable biofilms with high bioelectrochemical activity and revealing their inherent connection to power generation capabilities. Furthermore, a novel intermittent polarization technique—multi-electrode alternating intermittent polarization technology—was developed based on these derived biofilms. This approach enabled continuous system polarization through alternating electrode activation while maintaining intermittent polarization characteristics, demonstrating enhanced potential for improving both wastewater treatment efficiency and power generation performance in MFC systems. This methodology may represent a novel scaling strategy for MFC applications.

Supplementary Materials: The following supporting information can be downloaded at: https://www.mdpi.com/article/10.3390/environments13070396/s1, Scheme S1: the diagram of the proposed MSC.

Author Contributions: Conceptualization, J.J. and J.H.; Methodology, J.J. and J.H.; Validation, J.J. and J.H.; Formal analysis, J.J., J.H., X.X. and C.L.; Investigation, J.J., J.H., X.X. and C.L.; Resources, J.J., X.X. and C.L.; Data curation, J.J. and J.H.; Writing—original draft, J.J. and J.H.; Writing—review and editing, J.J., J.H., X.X. and C.L.; Project administration, J.J., J.H., X.X. and C.L.; Funding acquisition, J.J. and C.L. All authors have read and agreed to the published version of the manuscript.

Funding: We acknowledge financial support from the National Natural Science Foundation of China (Grant Nos. 21974097 and 22274117) and the Education Department of Guangdong Province (Grant No. 2022ZDJS027).

Data Availability Statement: The original contributions presented in the study are included in the article; further inquiries can be directed to the corresponding authors.

Conflicts of Interest: The authors declare no conflicts of interest. The funders had no role in the design of the study; in the collection, analyses, or interpretation of data; in the writing of the manuscript; or in the decision to publish the results.

References

1. Niu, Y.; Xue, D.; Dai, X.; Guo, G.; Yang, X.; Yang, L.; Bai, Z. Sustainable Power Generation from Sewage with Engineered Microorganisms as Electrocatalysts. *Nat. Sustain.* **2024**, *7*, 1182–1189. [CrossRef]
2. Song, Y.; Gu, P.; Liu, J.; Sun, H.; Cai, Z.; Li, J.; Xu, Z.; Li, Z.; Zou, J. Navigating the Developments of Air-Cathode Catalysts for Efficient and Sustainable Bio-Energy Production from Wastewater in Microbial Fuel Cells. *Coord. Chem. Rev.* **2024**, *517*, 216019. [CrossRef]
3. Yang, X.; He, H.; Lv, T.; Qiu, J. Fabrication of Biomass-Based Functional Carbon Materials for Energy Conversion and Storage. *Mater. Sci. Eng. R Rep.* **2023**, *154*, 100736. [CrossRef]
4. Kandpal, R.; Ali, S.W.; Ahammad, S.Z. Textile-Based Flexible Electrodes Enriching High Power Density Electroactive Biofilms Dominated by Lysinibacillus for Energy-Positive Textile Wastewater Remediation in Multielectrode Assembly Bioelectrochemical Systems. *Chem. Eng. J.* **2025**, *507*, 159947. [CrossRef]
5. Alkhawlani, Q.; Algburi, S.; Sabeeh, S.; Radwan, E.; Al Asmari, A.F.; Islam, S. Nitrogen-Doped Graphene/Carbon Felt Bioanode Enhances Power Generation in Microbial Fuel Cells. *Electrochem. Commun.* **2026**, *188*, 108172. [CrossRef]
6. You, J.; Ye, L.; Zhang, S.; Zhao, J.; Zhao, Y.; He, Y.; Chen, J.; Kennes, C.; Chen, D. Electrode Functional Microorganisms in Bioelectrochemical Systems and Its Regulation: A Review. *Biotechnol. Adv.* **2025**, *79*, 108521. [CrossRef] [PubMed]
7. Ayaz, K.; Zablocka-Godlewska, E.; Abdullah; Shakibania, S.; Patel, T.; Karon, K.; Krukiewicz, K. Enhancing Microbial Adhesion and Electron Transfer of *Shewanella oneidensis* MR-1 with Polyaniline-Glucose-Gelatin Coating for Bioelectrochemical Applications. *J. Environ. Chem. Eng.* **2026**, *14*, 121546. [CrossRef]
8. Liu, Y.; Harnisch, F.; Fricke, K.; Sietmann, R.; Schröder, U. Improvement of the Anodic Bioelectrocatalytic Activity of Mixed Culture Biofilms by a Simple Consecutive Electrochemical Selection Procedure. *Biosens. Bioelectron.* **2008**, *24*, 1006–1011. [CrossRef] [PubMed]
9. Wang, Y.Y.; Wang, Z.J.; Kong, X.Q.; Song, Y.; Tian, Y.; Lin, J. Capacitive and Biocompatibility Composite Anode Material for Enhanced Renewable Energy Conversion for MFCs. *Fuel* **2024**, *376*, 132736. [CrossRef]
10. Molderez, T.R.; Prévoteau, A.; Ceyssens, F.; Verhelst, M.; Rabaey, K. A Chip-Based 128-Channel Potentiostat for High-Throughput Studies of Bioelectrochemical Systems: Optimal Electrode Potentials for Anodic Biofilms. *Biosens. Bioelectron.* **2021**, *174*, 112813. [CrossRef] [PubMed]
11. Rossi, R.; Logan, B.E. Impact of External Resistance Acclimation on Charge Transfer and Diffusion Resistance in Bench-Scale Microbial Fuel Cells. *Bioresour. Technol.* **2020**, *318*, 123921. [CrossRef] [PubMed]
12. Zhang, X.; Prévoteau, A.; Louro, R.O.; Paquete, C.M.; Rabaey, K. Periodic Polarization of Electroactive Biofilms Increases Current Density and Charge Carriers Concentration While Modifying Biofilm Structure. *Biosens. Bioelectron.* **2018**, *121*, 183–191. [CrossRef] [PubMed]
13. Ter Heijne, A.; Pereira, M.A.; Pereira, J.; Sleutels, T. Electron Storage in Electroactive Biofilms. *Trends Biotechnol.* **2021**, *39*, 34–42. [CrossRef] [PubMed]
14. Pereira, J.; Neves, P.; Nemanic, V.; Pereira, M.A.; Sleutels, T.; Hamelers, B.; ter Heijne, A. Starvation Combined with Constant Anode Potential. Triggers Intracellular Electron. Storage in Electro-Active Biofilms. *Water Res.* **2023**, *242*, 120278. [CrossRef] [PubMed]
15. Zhang, X.; Rabaey, K.; Prévoteau, A. Reversible Effects of Periodic Polarization on Anodic Electroactive Biofilms. *ChemElectroChem* **2019**, *6*, 1921–1925. [CrossRef]
16. Zhang, X.; Luther, A.K.; Rabaey, K.; Prévoteau, A. Periodic Polarization Duty Cycle Tunes Performance and Adhesion of Anodic Electroactive Biofilms. *Bioelectrochemistry* **2024**, *155*, 108581. [CrossRef] [PubMed]
17. Yang, W.; Kim, K.-Y.; Saikaly, P.E.; Logan, B.E. The Impact of New Cathode Materials Relative to Baseline Performance of Microbial Fuel Cells All with the Same Architecture and Solution Chemistry. *Energy Environ. Sci.* **2017**, *10*, 1025–1033. [CrossRef]
18. Wu, T.; Gao, Y.; Zhang, T.Y.; Wen, Q.; Chen, Y.; Lin, C.G.; Qiu, Z.H. Synergistic S/Se-co-Doped FeMn-N-C Electrocatalyst for High-Efficiency Bioenergy Conversion in Microbial Fuel Cells. *J. Appl. Electrochem.* **2026**, *56*, 95. [CrossRef]

19. Yanuka-Golub, K.; Reshef, L.; Rishpon, J.; Gophna, U. Specific Desulfuromonas Strains Can Determine Startup Times of Microbial Fuel Cells. *Appl. Sci.* **2020**, *10*, 8570. [CrossRef]
20. Ren, Z.; Ji, G.; Liu, H.; Yang, M.; Xu, S.; Ye, M.; Lichtfouse, E. Accelerated Start-up and Improved Performance of Wastewater Microbial Fuel Cells in Four Circuit Modes: Role of Anodic Potential. *J. Power Sources* **2022**, *535*, 231403. [CrossRef]
21. Fathima, A.; Zoqratt, M.Z.H.b.M.; Lim, S.Y.; Ling, F.Y.; Chong, M.N. Influence of Ferric Oxides with Varying Crystallinity on the Enrichment of Halophilic Exoelectrogens: An Application for Power Generation in Microbial Fuel Cells. *J. Water Process Eng.* **2023**, *56*, 104458. [CrossRef]
22. Jung, S.P.; Son, S.; Koo, B. Reproducible Polarization Test Methods and Fair Evaluation of Polarization Data by Using Interconversion Factors in a Single Chamber Cubic Microbial Fuel Cell with a Brush Anode. *J. Clean. Prod.* **2023**, *390*, 136157. [CrossRef]
23. Sindhuja, M.; Sudha, V.; Harinipriya, S. Insights on the Resistance, Capacitance and Bioelectricity Generation of Microbial Fuel Cells by Electrochemical Impedance Studies. *Int. J. Hydrogen Energy* **2019**, *44*, 5428–5436. [CrossRef]
24. Peng, X.; Yu, H.; Yu, H.; Wang, X. Lack of Anodic Capacitance Causes Power Overshoot in Microbial Fuel Cells. *Bioresour. Technol.* **2013**, *138*, 353–358. [CrossRef] [PubMed]
25. Hong, Y.; Call, D.F.; Werner, C.M.; Logan, B.E. Adaptation to High Current Using Low External Resistances Eliminates Power Overshoot in Microbial Fuel Cells. *Biosens. Bioelectron.* **2011**, *28*, 71–76. [CrossRef] [PubMed]
26. Yu, F.; Wang, C.; Ma, J. Capacitance-Enhanced 3D Graphene Anode for Microbial Fuel Cell with Long-Time Electricity Generation stability. *Electrochim. Acta* **2018**, *259*, 1059–1067. [CrossRef]
27. Bonanni, P.S.; Schrott, G.D.; Robuschi, L.; Busalmen, J.P. Charge Accumulation and Electron Transfer Kinetics in Geobacter Sulfurreducens Biofilms. *Energy Environ. Sci.* **2012**, *5*, 6188–6195. [CrossRef]
28. Koók, L.; Nemestóthy, N.; Bélafi-Bakó, K.; Bakonyi, P. The Influential Role of External Electrical Load in Microbial Fuel Cells and Related Improvement Strategies: A Review. *Bioelectrochemistry* **2021**, *140*, 107749. [CrossRef] [PubMed]
29. Cheng, K.Y.; Ho, G.; Cord-Ruwisch, R. Affinity of Microbial Fuel Cell Biofilm for the Anodic Potential. *Environ. Sci. Technol.* **2008**, *42*, 3828–3834. [CrossRef] [PubMed]
30. Scarabotti, F.; Rago, L.; Bühler, K.; Harnisch, F. The Electrode Potential Determines the Yield Coefficients of Early-Stage Geobacter Sulfurreducens Biofilm Anodes Geobacter Sulfurreducens. *Bioelectrochemistry* **2021**, *140*, 107752. [CrossRef] [PubMed]
31. Torres, C.I.; Krajmalnik-Brown, R.; Parameswaran, P.; Marcus, A.K.; Wanger, G.; Gorby, Y.A.; Rittmann, B.E. Selecting Anode-Respiring Bacteria Based on Anode Potential: Phylogenetic, Electrochemical, and Microscopic Characterization. *Environ. Sci. Technol.* **2009**, *43*, 9519–9524. [CrossRef] [PubMed]
32. Yang, G.; Huang, L.; Yu, Z.; Liu, X.; Chen, S.; Zeng, J.; Zhou, S.; Zhuang, L. Anode Potentials Regulate Geobacter Biofilms: New Insights from the Composition and Spatial Structure of Extracellular Polymeric Substances. *Water Res.* **2019**, *159*, 294–301. [CrossRef] [PubMed]
33. Dziegielowski, J.; Metcalfe, B.; Di Lorenzo, M. Towards Effective Energy Harvesting from Stacks of Soil Microbial Fuel Cells. *J. Power Sources* **2021**, *515*, 230591. [CrossRef]
34. Alaraj, M.; Park, J.-D. Net Power Positive Maximum Power Point Tracking Energy Harvesting System for Microbial Fuel Cell. *J. Power Sources* **2019**, *418*, 225–232. [CrossRef]
35. Maye, S.; Delabays, L.; Sansonnens, J.; Blatter, M.; Huguenin, G.; Fischer, F. Computerized Voltage Reversal Prevention in Second and Third Year 1000-Liter Microbial Fuel Cell. *Renew. Sustain. Energy Rev.* **2025**, *208*, 115017. [CrossRef]
36. Taufemback, W.F.; Hotza, D.; de Recouvreux, D.O.S.; Calegari, P.C.; Pineda-Vásquez, T.G.; Antônio, R.V.; Watzko, E.S. Techniques for Obtaining and Mathematical Modeling of Polarization Curves in Microbial Fuel Cells. *Mater. Chem. Phys.* **2024**, *315*, 128998. [CrossRef]
37. Logan, B.E.; Rossi, R.; Ragab, A.; Saikaly, P.E. Electroactive Microorganisms in Bioelectrochemical Systems. *Nat. Rev. Microbiol.* **2019**, *17*, 307–319. [CrossRef] [PubMed]
38. Commault, A.S.; Lear, G.; Packer, M.A.; Weld, R.J. Influence of Anode Potentials on Selection of Geobacter Strains in Microbial Electrolysis Cells Geobacter. *Bioresour. Technol.* **2013**, *139*, 226–234. [CrossRef] [PubMed]
39. Zhu, Q.; Hu, J.; Liu, B.; Liang, S.; Xiao, K.; Yu, W.; Yuan, S.; Yang, J.; Hou, H. Potassium Channel Blocker Selectively Enriched Geobacter from Mixed-Cultured Electroactive Biofilm: Insights from Microbial Community, Functional Prediction and Gene Expressions Geobacte. *Bioresour. Technol.* **2022**, *364*, 128109. [CrossRef] [PubMed]
40. Commault, A.S.; Barrière, F.; Lapinsonnière, L.; Lear, G.; Bouvier, S.; Weld, R.J. Influence of Inoculum and Anode Surface Properties on the Selection of Geobacter-Dominated Biofilms Geobacter. *Bioresour. Technol.* **2015**, *195*, 265–272. [CrossRef] [PubMed]
41. Zhu, X.; Tokash, J.C.; Hong, Y.; Logan, B.E. Controlling the Occurrence of Power Overshoot by Adapting Microbial Fuel Cells to High Anode Potentials. *Bioelectrochemistry* **2013**, *90*, 30–35. [CrossRef] [PubMed]
42. Chatterjee, P.; Dessì, P.; Kokko, M.; Lakaniemi, A.-M.; Lens, P. Selective Enrichment of Biocatalysts for Bioelectrochemical Systems: A Critical Review. *Renew. Sustain. Energy Rev.* **2019**, *109*, 10–23. [CrossRef]

43. Raghavulu, S.V.; Babu, P.S.; Goud, R.K.; Subhash, G.V.; Srikanth, S.; Mohan, S.V. Bioaugmentation of an Electrochemically Active Strain to Enhance the Electron Discharge of Mixed Culture: Process Evaluation through Electro-Kinetic Analysis. *RSC Adv.* **2011**, *2*, 677–688. [CrossRef]
44. Elgrishi, N.; Rountree, K.J.; McCarthy, B.D.; Rountree, E.S.; Eisenhart, T.T.; Dempsey, J.L. A Practical Beginner's Guide to Cyclic Voltammetry. *J. Chem. Educ.* **2018**, *95*, 197–206. [CrossRef]

Disclaimer/Publisher's Note: The statements, opinions and data contained in all publications are solely those of the individual author(s) and contributor(s) and not of MDPI and/or the editor(s). MDPI and/or the editor(s) disclaim responsibility for any injury to people or property resulting from any ideas, methods, instructions or products referred to in the content.